Effect of Surface Structures on Droplet Impact Over Flat and Cylindrical Surfaces

Saptaparna Patra, Avik Saha, and Arup Kumar Das

1 Introduction

The lotus leaf has unique superhydrophobic and self-cleaning characteristics [1]. This attribute of the lotus leaf has subsequently been used to fabricate artificial surfaces which can display similar superhydrophobic and self-cleaning properties. Thus, the wetting of superhydrophobic surfaces has attracted a lot of research work in recent years. Researchers have fabricated many superhydrophobic surfaces with contact angles greater than 150° [2]. The chemical and physical properties of the solid substrate have an important role in deciding the droplets' behavior after the impact [3]. Introducing textures on the substrate can also influence the movement of the droplet [4]. With the advent of new manufacturing technologies and microfabrication, it has also become possible to fabricate complex superhydrophobic substrate structures [5]. Droplet dynamics are largely governed by an interplay between the inertia effects during the initial impact, followed by which the viscous and surface tension forces become more dominant. This interplay continues till equilibrium is achieved between these forces [6]. Generally, the superhydrophobic property of structured surfaces can be attributed to the air trapped in between the structures, which reduces the inertia effect of the droplet during impact. However, when the droplet impacts with a high enough energy, it can remove the trapped air, neutralizing the superhydrophobicity to some extent [7].

Due to the wide-ranging occurrences and applications of droplet impact in nature, it becomes essential to be able to model the dynamics optimally. One of the most common droplet impact studies applications is spray cooling, which allows high heat transfer rates, and is predominant in the electronics and semiconductor industries [8].

S. Patra
Department of Mechanical Engineering, NIT Durgapur, Durgapur 713209, India

A. Saha (✉) · A. K. Das
Department of Mechanical and Industrial Engineering, IIT Roorkee, Roorkee 247667, India
e-mail: aviksaha129@gmail.com

K. M. Singh et al. (eds.), *Fluid Mechanics and Fluid Power, Volume 5*, Lecture Notes in Mechanical Engineering, https://doi.org/10.1007/978-981-99-6074-3_17

The anti-icing properties of the superhydrophobic surfaces can also be utilized in colder climates, especially for power transmission equipment and aerospace industries [9–11]. Some other commonly encountered applications of droplet dynamics include wetting during fuel injection [12, 13], inkjet printing [14], anti-corrosion [15], pesticide spraying [16], and many more.

2 Literature Review and Objective

Two main wetting phenomena are observed during droplet impact on structured surfaces. The droplet penetrates the entire structured geometry by expelling the air, which is the Wenzel State [17]. When the droplet rests on the structured surface, not wholly penetrating the gaps, it is known as the Cassie–Baxter state [18]. Bhardwaj et al. experimentally studied the droplet impact hydrodynamics on flat and micropillar hydrophobic surfaces and observed non-bouncing, partial bouncing, and complete bouncing as possible outcomes and the transition from the Cassie–Baxter state to the Wenzel State. [19].

Many researchers have experimentally studied droplet impact on superhydrophobic flat and curved surfaces. It was experimentally observed that the impact velocity of the droplet on the superhydrophobic surface has an important role in the subsequent droplet morphologies [20]. Antonini et al. found that the droplet spreading time is independent of the impact velocity for moderate Weber numbers, with the surface contact angle being the more decisive factor [21]. Experimental investigation of droplet impact on solid surfaces has revealed six possible outcomes: deposition, prompt splash, corona splash, receding breakup, partial rebound, and complete rebound [22]. Ding et al. studied the droplet impact on a superhydrophobic surface with a single circular pillar and reported droplet rebound and splashing for various values of Weber numbers [23]. Li et al. numerically simulated droplet impact on a flat solid superhydrophobic surface and observed a doughnut-shaped breakup regime [24]. A relationship between molecular dynamics and experimental investigation of droplet impact on a pillared superhydrophobic surface. They observed that the impact velocity does not affect the contact time from 0.31 to 1.71 m/s. [25]. Abolghasemezaki et al. experimented on droplet impact on structured cylindrical surfaces to reduce contact time, which was independent of the impact velocity [26]. Khojasteh et al. observed the impact on flat and spherical superhydrophobic surfaces. They found that the predicted spreading factor followed the experimental results for flat surfaces but not spherical ones [27]. A more comprehensive review of recent advances in droplet hydrodynamics on a superhydrophobic surface can be found in [28].

The main objective of this paper is to study the hydrodynamics of a droplet after its impact on flat and cylindrical structured surfaces. Gauthier et al. have investigated the impact of a water droplet on superhydrophobic textured surfaces employing experimental techniques. They used a nickel wire on a polished aluminum surface to generate a superhydrophobic surface with stripes [29]. Many studies have also

observed the effects of a superhydrophobic pillared surface [30–32] on the droplet dynamics, but correlation and comparison between them are rare in literature. Similarly, many researchers have studied the droplet impact on cylindrical structured surfaces, but no comparison exists between them.

In this paper, we have numerically simulated the impact of a droplet on a hydrophobic flat and cylindrical surface and then the same surfaces with pillars and stripes, thus rendering the surfaces superhydrophobic.

3 Materials and Methods

3.1 Mathematical Modeling

The Volume of Fluid (VOF) approach has been used to trace the droplet's movement after its impact on the hydrophobic surfaces. VOF is a well-established modeling method that effectively tracks the interface of the phases. To model the drop impact, the conservation of momentum (Eq. 1) and conservation of mass (Eq. 2) equations for incompressible fluid have been solved using the framework of OpenFOAM. The volumetric surface tension force has been accounted for in the source term of the momentum equation

$$\frac{\partial \rho}{\partial t} + \nabla.(\rho \boldsymbol{u}) = 0 \tag{1}$$

$$\frac{\partial (\rho \boldsymbol{u})}{\partial t} + \nabla.(\rho \boldsymbol{u}\boldsymbol{u}) = \nabla.\left(\mu\left(\nabla \boldsymbol{u}^T + \nabla \boldsymbol{u}\right)\right) - \nabla p + \rho g + F_s \tag{2}$$

The volumetric surface tension is calculated using the Continuum Surface Tension model as depicted in Eq. 3, where σ is the coefficient of surface tension and κ is the mean curvature of the free surface (Eq. 4).

$$F_s = \sigma \kappa \nabla \alpha \tag{3}$$

$$\kappa = -\nabla.\left(\frac{\nabla \alpha}{|\nabla \alpha|}\right) \tag{4}$$

In the VOF model, the volume fraction (α) is used to capture the interface. The $\alpha = 1$ denotes a water-filled cell, and $\alpha = 0$ denotes an air-filled cell. This α is solved from the. VOF advection equation as depicted in Eq. 5. All the thermophysical properties, such as density and viscosity, are calculated using the phase fraction equation as depicted in Eq. 6 and 7. The various properties of the phases are shown in Table 1.

Table 1 Properties of the phases

Phase	Viscosity	Density	Surface Tension
Water	0.00089 Pa s	998 kg/m^3	0.07 N/m
Air	1.81e-5 Pa s	1.225 kg/m^3	

$$\frac{\partial \alpha}{\partial t} + \nabla.(\alpha \boldsymbol{u}) = 0 \tag{5}$$

$$\rho = \alpha \rho_{\text{liquid}} + (1 - \alpha)\rho_{\text{gas}} \tag{6}$$

$$\mu = \alpha \mu_{\text{liquid}} + (1 - \alpha)\mu_{\text{gas}} \tag{7}$$

3.2 Geometric Modeling

Several geometries were modeled for our study. A spherical droplet of water is dropped on a solid substrate (flat and curved) with an initial velocity (Fig. 1a, b). The initial velocity was set so that the impact velocity was 1 m/s. On the flat surfaces, two different structures, pillars, and stripes were added, and the results were subsequently compared with a hydrophobic plain flat surface. The initial spherical droplet diameter for the flat surfaces was assumed to be 1.6 mm. A spherical droplet of diameter D_0 = 2.4 mm was dropped on the curved surfaces of diameter D = 4 mm. The ratio of the diameters D^* is fixed as 1.67. Three different structured curved surfaces were studied: pillared, circumferential stripes, and axial stripes, as shown in Fig. 1, and the corresponding results were compared with that of a hydrophobic curved surface without any structures. The equilibrium contact angle was set at 120°.

3.3 Validation of Numerical Model

Experimental data obtained by Wang et al. [33] has been used to verify the solution methodology and the accuracy of our model. Here we compare the droplet morphologies as obtained experimentally with our numerical model. A similar validation has also been performed by Khojasteh et al. [27]. The model has been set up using a droplet radius of 1 mm, which impacts the superhydrophobic surface (with a static contact angle of 163 degrees) with a velocity of 0.56 m/s. The Weber number is 4.36. As observed in the experiment, the droplet flattens into a pancake shape upon impact and then retracts and rebounds, thus confirming our numerical simulations. The morphology comparisons are shown in Fig. 2, and they appear to be in good agreement.

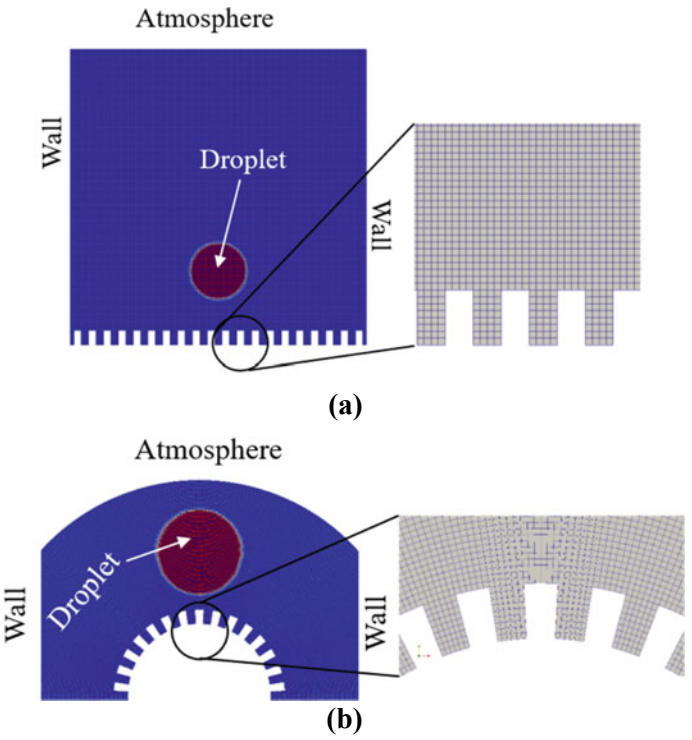

Fig. 1 Geometry, domain discretization, and boundary conditions for **a** flat structured surface and **b** cylindrical structured surface

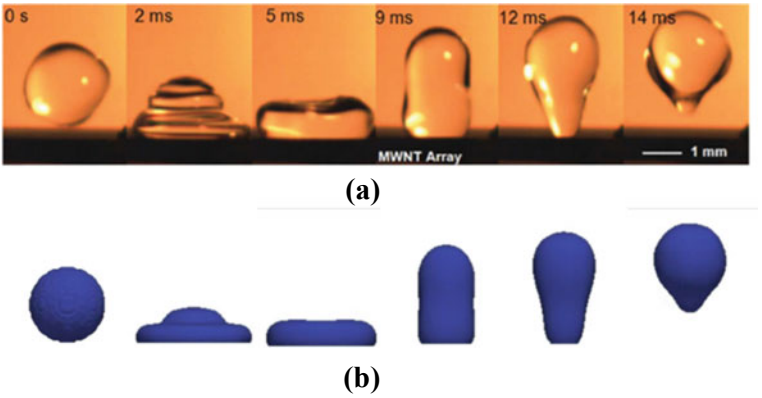

Fig. 2 **a** Experimental investigation by Wang et al. [33]. **b** Numerical simulation results obtained by our model

4 Results and Discussion

4.1 Impact of Droplet on Structured Flat Surfaces

Upon impact of the droplet on the flat structured substrate, we observed a complete rebound in both the cases (Striped and Pillared), whereas, on the plain hydrophobic surface, we obtained a partial rebound (which is per what has been reported in the literature [34]) (Fig. 3c). When the droplet strikes the surface, the kinetic energy is converted into interfacial energy and viscous dissipation, and the droplet starts to spread. However, the viscous dissipation can be neglected as we deal with the droplet on a millimeter scale. The structures then obstruct this spreading. The droplet on the pillared surface initially deforms and forms a multi-layered pancake-like structure (2 ms) by completely impinging the gaps between the pillars (Wenzel State) (Fig. 3a). In the striped surface, such a pancake-like structure is not seen; instead, the droplet cannot completely impinge the gaps after 2 ms (Transition between the Wenzel and Cassie-Baxter States). The droplet spreads to a maximum diameter at the 3 ms mark, which begins to retract on both surfaces.

Interestingly, an air pocket is observed during the retraction stages on both surfaces, which is more prominent on the striped surface (Fig. 3b). The main forces behind the retraction of the droplet are the surface tension and capillary forces. On the flat hydrophobic surface, the droplet spreads symmetrically.

The spreading is intuitively higher on the flat surface because there are no obstructions. The droplet spreading in the transverse (henceforth referred to as the X-Direction) and the direction into the plane (henceforth referred to as the Z-direction) of Fig. 3, for the pillared surface, is also symmetrical. The spreading in the X-direction in the pillared surface is more than the striped surface because of the unrestricted passage of the droplet over the pillars. Because the stripes prevent spreading in the X-Direction, the spreading is more in the Z-Direction on the striped surface.

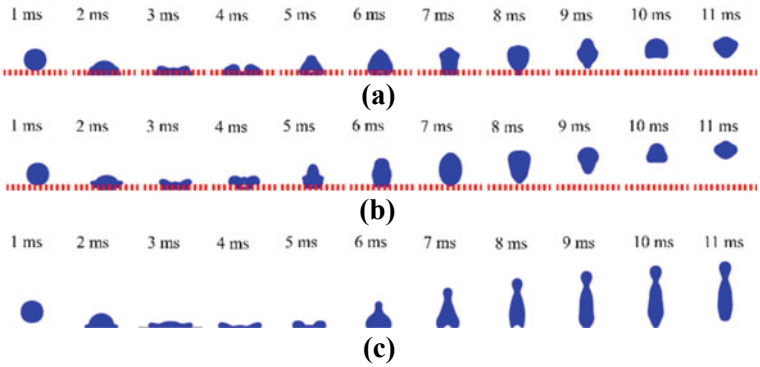

Fig. 3 Front view of **a** Droplet impact on the pillared surface. **b** Droplet impact on the striped surface. **c** Droplet impact on the plain hydrophobic surface

The spreading in the X and Z-Directions with time for the three surfaces have been depicted in Fig. 4b, c, respectively. The spreading during the initial impact is quantified using the normalized maximum spreading diameter (D_{max}/D_0). The normalized diameter at any instant is calculated as the ratio between instantaneous droplet diameter and the original droplet diameter (D_0). The post-impact bouncing dynamics are shown in Fig. 4d. After reaching the maximum spreading diameter, the droplets start to retract as the surface energy begins to convert into kinetic energy., thus giving the droplet an upward velocity, and the droplet rebounds from the surface. After subsequent bounces, as more and more energy is dissipated to the surface, the droplet's rebound height reduces (Fig. 4a). This rebound height is highest for the plain surface, followed by the striped and pillared surfaces, and this can be attributed to the fact that the highest amount of energy is dissipated as surface energy during the impact on the pillared surface. The contact time with the surface and the structures is highest for the plain hydrophobic surface, followed by the pillared and striped surface.

4.2 Impact of Droplet on Structured Cylindrical Surfaces

When the droplet impacts the structured cylindrical surface, we observe two main phenomena: complete rebound and partial rebound with droplet splitting. The four geometries under investigation are a hydrophobic cylinder, cylinder with axial stripes, cylinder with circumferential stripes, and cylinder with pillars. The droplet morphologies at various time stamps are shown in figure. It is shown that on the cylindrical pillared surface, a complete rebound occurs. On the axially and circumferentially striped cylinders, as well as on the hydrophobic cylinder, rebound with droplet splitting is observed. During the impact, the major forces involved are gravity, inertial, and surface tension forces. The effects of viscous dissipation are neglected again due to the size of the droplet. Since the diameter of the cylinder is larger than the initial diameter of the droplet, the droplet cannot completely encompass the cylinder in the azimuthal direction. Hence, upon spreading the droplet overhangs the cylinder, maintaining downward inertia. Subsequently, when the droplet starts retracting, the middle region of the droplet gains kinetic energy upward, whereas the overhanging parts have downward inertia, thus stretching the droplet. When this stretching overcomes the surface tension, the droplet splits.

In the case of the cylinder with the axial stripes, the droplet stretches in the axial direction more than the azimuthal direction. This causes an earlier splitting (Figs. 5b, 6b). In the cylinder with circumferential stripes, the obstruction prevents stretching in the axial direction, and hence more spreading is observed in the azimuthal direction. This brings about splitting a little later (during the rebound) (Figs. 5c, 6c). The split droplets later recombine. In the cylinder with pillars, the availability of space allows the droplet to spread more evenly, leading to lesser stretching; hence, no splitting is observed. In the plain hydrophobic cylinder, the spreading occurs symmetrically. It is observed that the angle of wrap around the cylinder increases with time. The

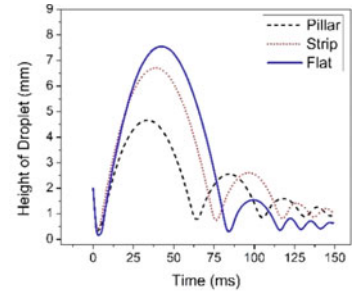

(a)

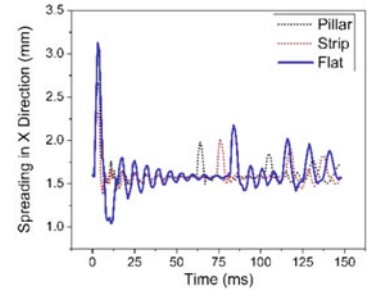

(b)

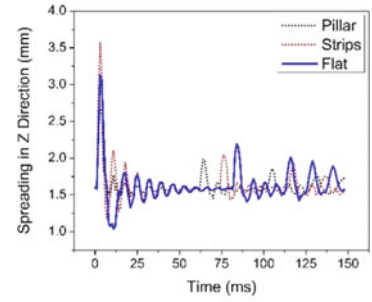

(c)

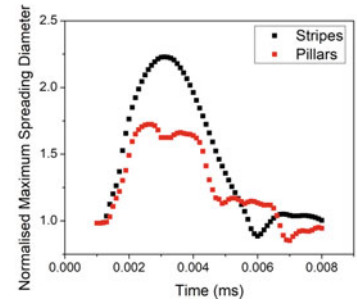

(d)

Fig. 4 **a** Height of the droplet. **b** Spreading in X-Direction. **c** Spreading in Z-Direction. **d** Normalised maximum spreading diameter

reason behind it is that the droplet has split, and the split droplets move downwards in opposite directions. A similar observation can be made for the axial strips. Whereas for the circumferential strips, since the droplet splitting occurs during rebound, the wrap angle keeps decreasing as the droplet bounces back. In the pillared surface, no splitting is observed, and the droplet usually bounces back, and hence the angle of wrap decreases (Fig. 7a). The height of the droplet is depicted in Fig. 7b. It is observed for the hydrophobic cylinder and the axially striped cylinder that after impact, the height of the droplet reduces. This is because the split droplets fall down under the effect of gravity. On the other hand, the droplets split during the rebound period and later recombine for the circumferentially striped cylinder, which is why the height increases. For the pillared cylinder, no splitting is observed, the droplet rebounds and the height keeps increasing. The contact times with the surface are also observed to be the highest for the pillared cylinder and the hydrophobic cylinder, followed by the axially striped cylinder, and lowest for the circumferentially striped cylinder. Interestingly, the droplet cannot penetrate the structures in the axially striped cylinder and remains at a transition between the Cassie-Baxter and Wenzel states.

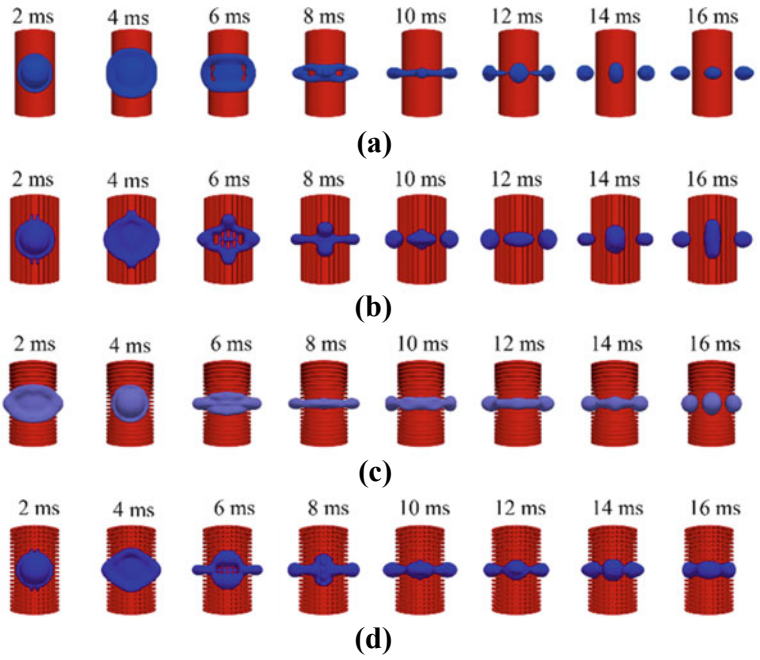

Fig. 5 Top view of impact on **a** Hydrophobic cylinder. **b** Cylinder with axial stripes, **c** Cylinder with circumferential stripes. **d** Cylinder with pillars

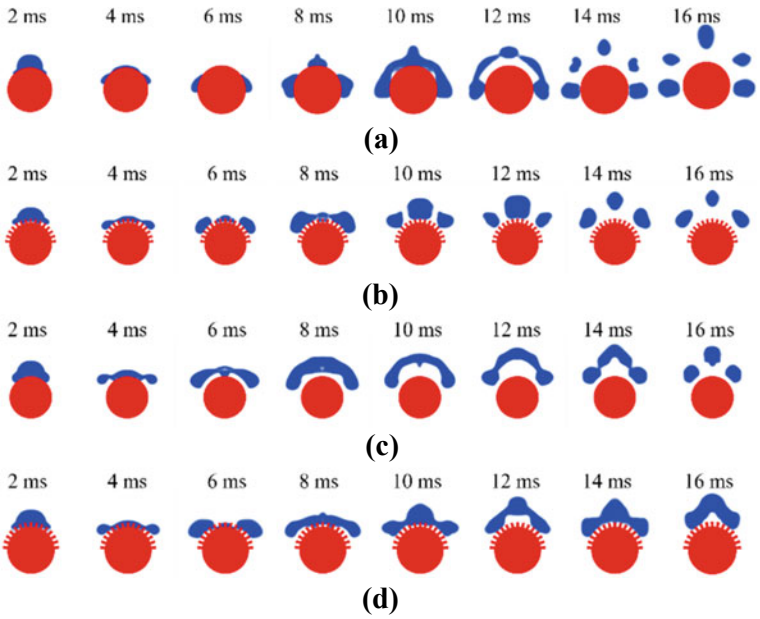

Fig. 6 Front view of the impact on **a** Hydrophobic cylinder. **b** Cylinder with axial stripes. **c** Cylinder with circumferential stripes. **d** Cylinder with pillars

5 Conclusion

In this present work, an effort is made to study the droplet impact dynamics on flat and cylindrical structured surfaces. Numerical simulations have been performed using OpenFOAM. The presence of structures on the hydrophobic surfaces effectively renders the surfaces superhydrophobic. We have studied a striped and pillared flat surface and compared the resulting dynamics with a plain hydrophobic surface. It is observed that the structures obstruct spreading: they promote spreading in the direction of the stripes and restrict it in the transverse direction. The pillars, on the other hand, prevent spreading symmetrically. Thus in the pillars, the spreading is symmetrical. The contact time of the droplet with the surface is observed to be higher for the pillared surface than the striped surface, and thus we can also conclude that a higher amount of energy is dissipated to the pillared surface than the striped surface. The contact time with the hydrophobic flat surface is the highest. During the initial impact, the droplet completely impinges the gaps between the structures (Wenzel State), which later transitions into the Cassie-Baxter state during subsequent impacts after bouncing. The splitting of droplets on plain and structured cylindrical surfaces is also investigated. The droplet is split in all three geometries except for the pillared cylinder. The contact time is also the highest for the pillared cylinder. Interestingly, splitting is observed on the circumferentially striped cylinder, and the split droplets recombine later on rebound.

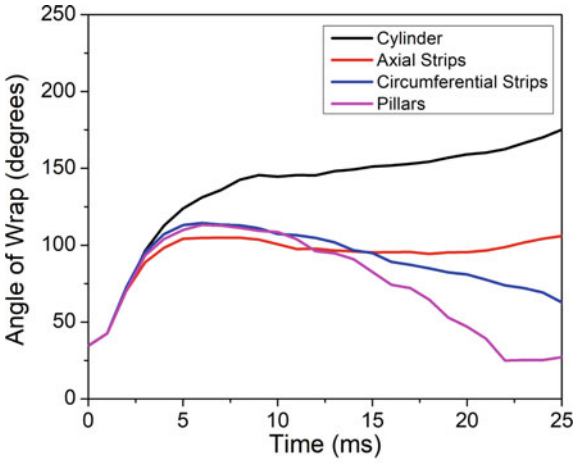

(a)

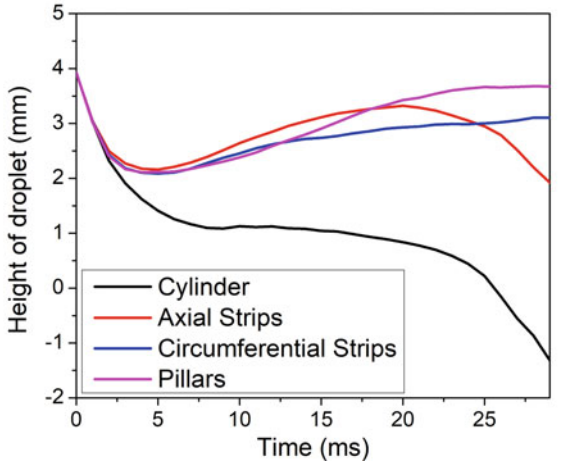

(b)

Fig. 7 **a** Angle of wrap around the cylinder. **b** Height of the droplet with time

Nomenclature

ρ	Density of phase (kg/m^3)
μ	Viscosity of phase (Pa s)
α	Phase fraction (–)
D	Diameter of cylinder (mm)
D_0	Initial diameter of droplet (mm)
D_{max}	Maximum spreading diameter (mm)
D^*	Diameter ratio D/D_0
u	Velocity (m/s)

g Accelaration due to gravity (m/s^2)
σ Coefficient of Surface tension (N/m)
F_s Force due to surface tension (N)
κ Mean curvature of free surface (–)

References

1. Barthlott W, Neinhuis C (1997) Purity of the sacred lotus, or escape from contamination in biological surfaces. Planta 202:1–8
2. Das S, Kumar S, Samal S, Mohanty S, Nayak S (2018) A review on superhydrophobic polymer nanocoatings: recent development and applications. Ind Eng Chem Res 57
3. Kannan R, Sivakumar D (2008) Impact of liquid drops on a rough surface comprising microgrooves. Exp Fluids 44:927–938
4. Malouin BA Jr, Koratkar NA, Hirsa AH, Wang Z (2010) Directed rebounding of droplets by microscale surface roughness gradients. Appl Phys Lett 96(23)
5. Wang D, Sun Q, Hokkanen MJ, Zhang C, Lin FY, Liu Q, Zhu SP, Zhou T, Chang Q, He B, Zhou Q (2020) Design of robust superhydrophobic surfaces. Nature 582:55–59
6. Bussmann M, Mostaghimi J (1999) On a three-dimensional volume tracking model of droplet impact. Phys Fluids 11:1406–1417
7. Shen Y, Tao J, Tao H, Chen S, Pan L, Wang T (2015) Relationship between wetting hysteresis and contact time of a bouncing droplet on hydrophobic surfaces. ACS Appl Mater Interfaces
8. Yan Z, Zhao R, Duan F, Wong T, Toh K, Choo K, Chan P, Chua Y (2011) Spray cooling
9. Sarkar D, Farzaneh M (2009) Superhydrophobic coatings with reduced ice adhesion. J Adhes Sci Technol 23:1215–1237
10. Wang N, Xiong D, Deng Y, Shi Y, Wang K (2015) Mechanically robust superhydrophobic steel surface with anti-icing. UV-durability, and corrosion resistance properties. ACS Appl Mater Interfaces
11. He H, Guo Z (2021) Superhydrophobic materials used for anti-icing Theory, application, and development. iScience 24
12. Liu YC, Farouk T, Savas AJ, Dryer FL, Avedisian CT (2013) On the spherically symmetrical combustion of methyl decanoate droplets and comparisons with detailed numerical modeling. Combust Flame 160:641–655
13. Moreira ALN, Moita AS, Panão M (2010) Advances and challenges in explaining fuel spray impingement: how much of single droplet impact research is useful. Progr Energy Combust Sci
14. Yusof A, Keegan H, Spillane CD, Sheils O, Martin C, O'Leary J, Zengerle R, Koltay P (2011) Inkjet-like printing of single-cells. Lab Chip 11:2447–2454
15. Vazirinasab E, Jafari R, Momen G (2017) Application of superhydrophobic coatings as a corrosion barrier: a review. Surface Coatings Technol
16. Massinon M, Lebeau F (2012) Experimental method for the assessment of agricultural spray retention based on high-speed imaging of drop impact on a synthetic superhydrophobic surface. Biosys Eng 112:56–64
17. Wenzel RN (1936) Resistance of solid surfaces to wetting by water. Ind Eng Chem 28(8):988–994
18. Cassie ABD, Baxter S (1944) Wettability of porous surfaces. Trans Faraday Soc 40:546–551
19. Patil N, Bhardwaj R, Sharma A (2015) Droplet impact dynamics on micropillared hydrophobic surfaces. Exp Thermal Fluid Sci 74
20. Tsai P, Pacheco S, Pirat C, Lefferts L, Lohse D (2009) Drop impact upon micro- and nanostructured superhydrophobic surfaces. Langmuir: ACS J Surfaces Colloids 25

21. Antonini C, Amirfazli A, Marengo M (2012) Drop impact and wettability: from hydrophilic to superhydrophobic surfaces. Phys Fluids 24
22. Rioboo R, Marengo M, Tropea C (2001) Outcomes from a drop impact on solid surfaces. Atom Sprays 11:155–166
23. Ding S, Hu Z, Dai L, Zhang X, Wu X (2021) Droplet impact dynamics on single-pillar superhydrophobic surfaces. Phys Fluids 33(10):102108
24. Li W, Wang J, Zhu C, Tian L, Zhao N (2021) Numerical investigation of droplet impact on a solid superhydrophobic surface. Phys Fluids 33(6):063310
25. Li H, Zhang K (2019) Dynamic behavior of water droplets impacting on the superhydrophobic surface: both experimental study and molecular dynamics simulation study. Appl Surf Sci 498:143793
26. Abolghasemibizaki M, McMasters RL, Mohammadi R (2018) Towards the shortest possible contact time: droplet impact on cylindrical superhydrophobic surfaces structured with macro-scale features. J Colloid Interface Sci 521:17–23
27. Khojasteh D, Bordbar A, Kamali R, Marengo M (2017) Curvature effect on droplet impacting onto hydrophobic and superhydrophobic spheres. Int J Comput Fluid Dyn 31:1–14
28. Khojasteh D, Kazerooni M, Salarian S, Kamali R (2016) Droplet impact on superhydrophobic surfaces: a review of recent developments: J Ind Eng Chem 42
29. Gauthier A, Symon S, Clanet C, Quéré D (2015) Water impacting on superhydrophobic macrotextures. Nat Commun 6:1–6
30. Zhang R, Farokhirad S, Lee T, Koplik J (2014) Multiscale liquid drop impact on wettable and textured surfaces. Phys Fluids 26(8):082003
31. Tsai P, Hendrix M, Dijkstra R, Shui L, Lohse D (2011) Microscopic structure influencing macroscopic splash at high Weber number. Soft Matter 7
32. Lee J, Hwang S-H, Yoon S-S, Khang D-Y (2019) Evaporation characteristics of water droplets in Cassie, Wenzel, and mixed states on superhydrophobic pillared Si surface. Colloids Surf A 562:304–309
33. Wang Z, Lopez C, Hirsa A, Koratkar N (2007) Impact dynamics and rebound of water droplets on superhydrophobic carbon nanotube arrays. Appl Phys Lett 91(2):023105
34. Parihar V, Chakraborty S, Das S, Chakraborty S, Dasgupta S (2020) Role of anisotropic pinning and liquid properties during partial rebound of droplets on unidirectionally structured hydrophobic surfaces. Chem Eng Sci 230